$D^{(*)}N$ interaction and the structure of $\Sigma_c(2800)$ and $\Lambda_c(2940)$ in chiral effective field theory

Bo Wang,[1,2,*] Lu Meng,[2,†] and Shi-Lin Zhu[2,1,‡]

[1]*Center of High Energy Physics, Peking University, Beijing 100871, China*
[2]*School of Physics and State Key Laboratory of Nuclear Physics and Technology, Peking University, Beijing 100871, China*

(Received 12 March 2020; accepted 15 May 2020; published 29 May 2020)

We study the DN and D^*N interactions to probe the inner structure of $\Sigma_c(2800)$ and $\Lambda_c(2940)$ with the chiral effective field theory to the next-to-leading order. We consider the contact term, one-pion-exchange and two-pion-exchange contributions to characterize the short-, long-, and mid-range interactions of the $D^{(*)}N$ systems. The low energy constants of the $D^{(*)}N$ systems are related to those of the $N\bar{N}$ interaction with a quark level Lagrangian that was inspired by the resonance saturation model. The $\Delta(1232)$ degree of freedom is also included in the loop diagrams. The attractive potential in the $[DN]^{I=1}_{J=1/2}$ channel is too weak to form a bound state, which indicates that the explanation of $\Sigma_c(2800)$ as the compact charmed baryon is more reasonable. Meanwhile, the potentials of the isoscalar channels are deep enough to yield the molecular states. We obtain the masses of the $[DN]^{I=0}_{J=1/2}$, $[D^*N]^{I=0}_{J=1/2}$, and $[D^*N]^{I=0}_{J=3/2}$ systems to be 2792.0, 2943.6, and 2938.4 MeV, respectively. The $\Lambda_c(2940)$ is probably the isoscalar D^*N molecule considering its low mass puzzle. Besides, the $\Lambda_c(2940)$ signal might contain the spin-$\frac{1}{2}$ and spin-$\frac{3}{2}$ two structures, which can qualitatively explain the significant decay ratio to D^0p and $\Sigma_c\pi$. We also study the $\bar{B}^{(*)}N$ systems and predict the possible molecular states in the isoscalar channels. We hope experimentalists could hunt for the open charmed molecular pentaquarks in the $\Lambda_c^+\pi^+\pi^-$ final state.

DOI: 10.1103/PhysRevD.101.094035

I. INTRODUCTION

Hadron spectroscopy plays an important role in understanding the low energy behaviors of QCD. The quark model is very successful in describing the hadron spectra [1]. But it is rather difficult to assign the near-threshold states, such as $X(3872)$ [2] and $D_{s0}(2317)$ [3], to the quark model predictions [4–9]. In the charmed baryon family, a state $\Lambda_c(2940)$ also falls into the same situation as the $X(3872)$ and $D_{s0}(2317)$.

In 2007, the *BABAR* Collaboration observed a charmed baryon $\Lambda_c(2940)$ in the D^0p invariant mass spectrum [10], which is an isosinglet since no signal is observed in the D^+p final state. It was subsequently confirmed by the Belle experiment in the decay mode $\Lambda_c(2940) \to \Sigma_c\pi$ [11]. In 2017, the J^P quantum numbers of $\Lambda_c(2940)$ were constrained by the LHCb measurement, and the most likely spin-parity assignment for $\Lambda_c(2940)$ is $J^P = \frac{3}{2}^-$ [12]. [The mass and width of $\Lambda_c(2940)$ obtained by the *BABAR*, Belle, and LHCb experiments are shown in Table I.]

Up until now, there are two different interpretations of the internal structure of $\Lambda_c(2940)$. One is the ordinal charmed baryon, and the other one is the D^*N molecular state. However, it is difficult to arrange $\Lambda_c(2940)$ to the $2P$ state in the charmed baryon spectroscopy, since its mass is about 60–100 MeV smaller than the calculations of the quark models [13–16]. Considering the $\Lambda_c(2940)$ lies about 6 MeV below the $D^{*0}p$ threshold, the molecular explanation was first proposed in Ref. [17], where the $\Lambda_c(2940)$ as the $\frac{1}{2}^-$ molecular state is preferred by analyzing its decay behaviors. In Ref. [18], He *et al.* studied the D^*N interaction with the one-boson-exchange model, and

TABLE I. The mass and width of $\Lambda_c(2940)$ in experiments (in units of MeV).

BABAR	$2939.8 \pm 1.3 \pm 1.0$	$17.5 \pm 5.2 \pm 5.9$
Belle	$2938.0 \pm 1.3^{+2.0}_{-4.0}$	13^{+8+27}_{-5-7}
LHCb	$2944.8^{+3.5}_{-2.5} \pm 0.4^{+0.1}_{-4.6}$	$27.7^{+8.2}_{-6.0} \pm 0.9^{+5.2}_{-10.4}$

*bo-wang@pku.edu.cn
†lmeng@pku.edu.cn
‡zhusl@pku.edu.cn

Published by the American Physical Society under the terms of the Creative Commons Attribution 4.0 International license. Further distribution of this work must maintain attribution to the author(s) and the published article's title, journal citation, and DOI. Funded by SCOAP³.

their calculation supports the interpretation of the $\Lambda_c(2940)$ as the D^*N bound state with $I(J^P) = 0(\frac{1}{2}^+)$ or $0(\frac{3}{2}^-)$. In Ref. [19], Ortega *et al.* investigated the $\Lambda_c(2940)$ as a D^*N molecule in the constituent quark model, and they obtain the binding solution in the isoscalar $J^P = \frac{3}{2}^-$ channel. In Refs. [20,21], the strong and radiative decays of $\Lambda_c(2940)$ are calculated in the molecular picture. A QCD sum rule study in Ref. [22] indicates the $\Lambda_c(2940)$ is not a compact state. Some recent calculations based on the chiral quark model also support the molecular explanation for $\Lambda_c(2940)$ [23,24]. (see Refs. [25–29] for review and Refs. [30–39] for other related works).

Another charmed baryon related with the DN threshold is $\Sigma_c(2800)$, which is an isotriplet and first observed by the Belle Collaboration in the $\Lambda_c\pi$ mass spectrum [40]. The neutral state $\Sigma_c(2800)^0$ was possibly confirmed by the *BABAR* experiment [41], but the measured mass from *BABAR* is about 50 MeV larger. The J^P of $\Sigma_c(2800)$ is still undetermined yet [1]. Like the $\Lambda_c(2940)$, $\Sigma_c(2800)$ is interpreted as the P-wave excitation of the charmed baryon in the λ mode [14,36,42–44], and DN molecule [22–24,45], respectively.

Investigating the DN and D^*N interaction is essential to disentangle the puzzles of $\Sigma_c(2800)$ and $\Lambda_c(2940)$. Besides, understanding the $D^{(*)}N$ interaction is also crucial to probe the D-mesic nuclei [46,47] and the properties of the charmed mesons in the nuclear matter [48,49]. An alternative approach based on the meson-exchange model [50] has been employed to construct the DN and $\bar{D}N$ interaction by the Jülich group [51–53].

Instead of the boson-exchange model, the modern theory of nuclear force is built upon the pioneering work of Weinberg [54,55] and largely developed in the framework of effective field theory. The chiral effective field theory was extensively exploited to study the NN interaction with great success [56–61]. The chiral effective field theory was also utilized to study the systems with heavy flavors in Refs. [62–68], which is a powerful tool in predicting the BB^* and B^*B^* bound states [64], reproducing the newly observed pentaquarks [66], extrapolating the $\Sigma_c N$ potential from the lattice QCD result to the physical pion mass [67], and so on. As a natural extension of the NN interaction, in this work, we use the chiral effective field theory to study the $D^{(*)}N$ interaction up to the next-to-leading order. We simultaneously consider the long-, mid-, and short-range interactions, and include the contribution of $\Delta(1232)$ in the loops as an intermediate state. With the chiral effective field theory, we calculate the $D^{(*)}N$ effective potentials and search for the possible bound states. The numerical results can be compared with the experimental data of $\Lambda_c(2940)$ and $\Sigma_c(2800)$ to see whether they are the genuine charmed baryons or the molecular nature.

This paper is organized as follows. In Sec. II, we give the Lagrangians and effective potentials of the $D^{(*)}N$ systems. In Sec. III, we illustrate our numerical results and discussions. In Sec. IV, we conclude with a short summary. In the Appendix we relate the low energy constants (LECs) to those of the $N\bar{N}$ system with a quark model.

II. LAGRANGIANS AND EFFECTIVE POTENTIALS

A. Effective chiral Lagrangians

We first show the leading order Lagrangian of the nucleon and pion interaction under the heavy baryon reduction [69], which reads

$$\mathcal{L}_{\mathcal{N}\varphi} = \bar{\mathcal{N}}(iv\cdot\mathcal{D} + 2g_a\mathcal{S}\cdot u)\mathcal{N}, \tag{1}$$

where $\mathcal{N} = (p, n)^T$ denotes the large component of the nucleon field under the nonrelativistic reduction. $v = (1, \mathbf{0})$ is the four-velocity of the nucleon and $\mathcal{D}_\mu = \partial_\mu + \Gamma_\mu$. $g_a \simeq 1.29$ is the axial-vector coupling constant. $\mathcal{S}^\mu = \frac{i}{2}\gamma_5\sigma^{\mu\nu}v_\nu$ stands for the spin operator of the nucleon. Γ_μ and u_μ are the chiral connection and axial-vector current, respectively. Their expressions read

$$\Gamma_\mu \equiv \frac{1}{2}[\xi^\dagger, \partial_\mu\xi] \equiv \tau^i\Gamma^i_\mu, \quad u_\mu \equiv \frac{i}{2}\{\xi^\dagger, \partial_\mu\xi\} \equiv \tau^i\omega^i_\mu, \tag{2}$$

where τ^i is the Pauli matrix,

$$\xi^2 = U = \exp\left(\frac{i\varphi}{f_\pi}\right), \qquad \varphi = \begin{bmatrix} \pi^0 & \sqrt{2}\pi^+ \\ \sqrt{2}\pi^- & -\pi^0 \end{bmatrix}, \tag{3}$$

and $f_\pi = 92.4$ MeV is the pion decay constant.

Considering the importance of $\Delta(1232)$ in the NN interaction [50,70–73], we adopt the small scale expansion method [74] to explicitly include the $\Delta(1232)$ in the Lagrangians. The Lagrangian that delineates the Δ-N-π coupling is given as

$$\mathcal{L}_{\Delta\varphi} = -\bar{\mathcal{T}}^\mu_i(iv\cdot\mathcal{D}^{ij} - \delta^{ij}\delta_a + 2g_1\mathcal{S}\cdot u^{ij})g_{\mu\nu}\mathcal{T}^\nu_j, \tag{4}$$

$$\mathcal{L}_{\Delta\mathcal{N}\varphi} = 2g_\delta(\bar{\mathcal{T}}^\mu_i g_{\mu\alpha}\omega^\alpha_i\mathcal{N} + \bar{\mathcal{N}}\omega^{\alpha\dagger}_i g_{\alpha\mu}\mathcal{T}^\mu_i), \tag{5}$$

where $\delta_a = m_\Delta - m_N$. $g_1 = \frac{9}{5}g_a$ is estimated with the quark model [74]. $g_\delta \simeq 1.05$ is the coupling constant for $\Delta N\pi$ vertex. $\mathcal{T}^\mu_i$ denotes the spin-$\frac{3}{2}$ and isospin-$\frac{3}{2}$ field $\Delta(1232)$ after performing the nonrelativistic reduction. Its matrix form reads

$$\mathcal{T}^1_\mu = \frac{1}{\sqrt{2}}\begin{bmatrix} \Delta^{++} - \frac{1}{\sqrt{3}}\Delta^0 \\ \frac{1}{\sqrt{3}}\Delta^+ - \Delta^- \end{bmatrix}_\mu,$$
$$\mathcal{T}^2_\mu = \frac{i}{\sqrt{2}}\begin{bmatrix} \Delta^{++} + \frac{1}{\sqrt{3}}\Delta^0 \\ \frac{1}{\sqrt{3}}\Delta^+ + \Delta^- \end{bmatrix}_\mu, \quad \mathcal{T}^3_\mu = -\sqrt{\frac{2}{3}}\begin{bmatrix} \Delta^+ \\ \Delta^0 \end{bmatrix}_\mu. \tag{6}$$

The leading order Lagrangian that depicts the interaction between the charmed mesons and light Goldstones reads [75,76]

$$\mathcal{L}_{\mathcal{H}\varphi} = i\langle \mathcal{H} v\cdot \mathcal{D}\bar{\mathcal{H}}\rangle - \frac{1}{8}\delta_b\langle \mathcal{H}\sigma^{\mu\nu}\bar{\mathcal{H}}\sigma_{\mu\nu}\rangle + g\langle \mathcal{H}\not{u}\gamma_5\bar{\mathcal{H}}\rangle, \quad (7)$$

where $\langle\cdots\rangle$ represents the trace in spinor space. δ_b is defined as $\delta_b = m_{D^*} - m_D$. $g \simeq -0.59$ stands for the axial coupling, whose sign is determined with the help of the quark model. The $\mathcal{H}$ is the superfield for the charmed mesons, which reads

$$\begin{aligned}\mathcal{H} &= \frac{1+\not{v}}{2}(P^*_\mu\gamma^\mu + iP\gamma_5),\\ \bar{\mathcal{H}} &= \gamma^0 H^\dagger\gamma^0 = (P^{*\dagger}_\mu\gamma^\mu + iP^\dagger\gamma_5)\frac{1+\not{v}}{2},\end{aligned} \quad (8)$$

with $P = (D^0, D^+)^T$ and $P^* = (D^{*0}, D^{*+})^T$, respectively. We construct the leading order contact Lagrangian to describe the short distance interaction between the nucleon and charmed meson,

$$\begin{aligned}\mathcal{L}_{\mathcal{NH}} = {} & D_a\bar{\mathcal{N}}\mathcal{N}\langle\bar{\mathcal{H}}\mathcal{H}\rangle + D_b\bar{\mathcal{N}}\gamma_\mu\gamma_5\mathcal{N}\langle\bar{\mathcal{H}}\gamma^\mu\gamma_5\mathcal{H}\rangle\\ & + E_a\bar{\mathcal{N}}\tau_i\mathcal{N}\langle\bar{\mathcal{H}}\tau_i\mathcal{H}\rangle + E_b\bar{\mathcal{N}}\gamma_\mu\gamma_5\tau_i\mathcal{N}\langle\bar{\mathcal{H}}\gamma^\mu\gamma_5\tau_i\mathcal{H}\rangle,\end{aligned} \quad (9)$$

where D_a, D_b, E_a, and E_b are four LECs. D_a and D_b contribute to the central potential and spin-spin interaction, respectively. E_a and E_b are related with the isospin-isospin interaction and contribute to the central and spin-spin interaction in spin space, respectively. With the quark model, we fix their values with the $N\bar{N}$ interaction as inputs, which is given in the Appendix.

B. Expressions of the effective potentials

In the framework of heavy hadron chiral perturbation theory, the scattering amplitudes of the $D^{(*)}N$ systems can be expanded order by order in powers of a small parameter $\varepsilon = q/\Lambda_\chi$, where q is either the momentum of Goldstone bosons or the residual momentum of heavy hadrons, and Λ_χ represents either the chiral breaking scale or the mass of a heavy hadron.[1] The expansion is organized by the power counting rule in Refs. [54,55]. The $\mathcal{O}(\varepsilon^0)$ Feynman diagrams for the DN and D^*N systems are shown in Fig. 1, which contain the contact and one-pion-exchange diagrams. The one-pion-exchange diagram for the DN system vanishes since the $DD\pi$ vertex is forbidden. The corresponding momentum-space potentials of the graphs in Fig. 1 read

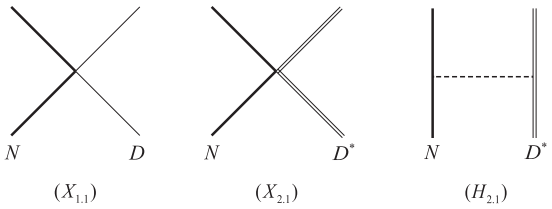

FIG. 1. The leading order Feynman diagrams that account for the $\mathcal{O}(\varepsilon^0)$ effective potentials of the ND ($X_{1,1}$), and ND^* ($X_{2,1}$, $H_{2,1}$) systems. We use the thick, thin, double-thin, and dashed lines to denote the N, D, D^*, and pion fields, respectively.

$$\mathcal{V}^{X_{1,1}}_{DN} = D_a - 4E_a(\mathbf{I}_1\cdot\mathbf{I}_2), \quad (10)$$

$$\mathcal{V}^{X_{2,1}}_{D^*N} = D_a + D_b\boldsymbol{\sigma}\cdot\mathbf{T} - 4(E_a + E_b\boldsymbol{\sigma}\cdot\mathbf{T})(\mathbf{I}_1\cdot\mathbf{I}_2), \quad (11)$$

$$\mathcal{V}^{H_{2,1}}_{D^*N} = (\mathbf{I}_1\cdot\mathbf{I}_2)\frac{gg_a}{f_\pi^2}\frac{(\boldsymbol{q}\cdot\boldsymbol{\sigma})(\boldsymbol{q}\cdot\mathbf{T})}{\boldsymbol{q}^2+m_\pi^2}, \quad (12)$$

where $\mathbf{I}_1$ and $\mathbf{I}_2$ are the isospin operators of D and N, respectively. The operators $\boldsymbol{\sigma}$ and $\mathbf{T}$ are related to the spin operators of the spin-$\frac{1}{2}$ baryon, spin-1 meson as $\frac{1}{2}\boldsymbol{\sigma}$ and $-\mathbf{T}$, respectively (see Ref. [66] for details). The Breit approximation

$$\mathcal{V}(\boldsymbol{q}) = -\frac{\mathcal{M}(\boldsymbol{q})}{\sqrt{2\Pi_i m_i 2\Pi_f m_f}} \quad (13)$$

is used to relate the scattering amplitude $\mathcal{M}(\boldsymbol{q})$ to the effective potential $\mathcal{V}(\boldsymbol{q})$ in momentum space (m_i and m_f are the masses of the initial and final states, respectively).

The next-to-leading order two-pion-exchange diagrams for the DN system are illustrated in Fig. 2. The effective potentials from these graphs read

$$\mathcal{V}^{F_{1,1}}_{DN} = (\mathbf{I}_1\cdot\mathbf{I}_2)\frac{1}{f_\pi^4}J^F_{22}(m_\pi, q), \quad (14)$$

$$\begin{aligned}\mathcal{V}^{T_{1,1}}_{DN} = {} & (\mathbf{I}_1\cdot\mathbf{I}_2)\frac{g^2}{f_\pi^4}\Big[(d-1)J^T_{34}\\ & - \boldsymbol{q}^2(J^T_{24}+J^T_{33})\Big](m_\pi, \mathcal{E}-\delta_b, q),\end{aligned} \quad (15)$$

$$\begin{aligned}\mathcal{V}^{T_{1,2}}_{DN} = {} & (\mathbf{I}_1\cdot\mathbf{I}_2)\frac{4g_\delta^2}{3f_\pi^4}\Big[(2-d)J^T_{34}\\ & - \boldsymbol{q}^2\frac{2-d}{d-1}(J^T_{24}+J^T_{33})\Big](m_\pi, \mathcal{E}-\delta_a, q),\end{aligned} \quad (16)$$

[1]The mass splitting $\delta_b \sim m_\pi$, so δ_b/Λ_χ can be safely treated as the small parameter in chiral expansions. However, the mass difference $\delta_a \sim 2m_\pi \ll m_N$, so strictly speaking, the "small parameter" δ_a/Λ_χ therefore has to be regarded as a *phenomenological* one. With the current accuracy, expanding to $(\delta_a/\Lambda_\chi)^2$ at the one-loop level can fulfill the convergence of the chiral expansions.

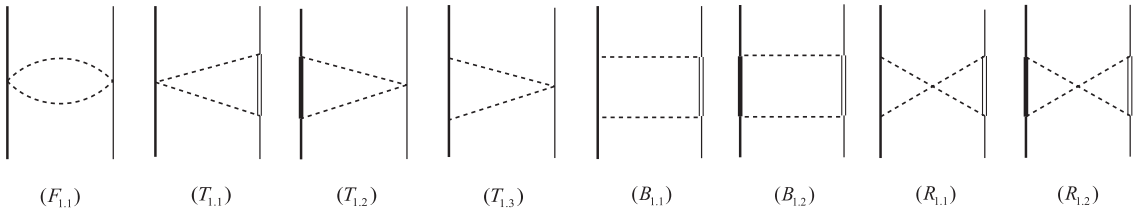

FIG. 2. The two-pion-exchange diagrams of the DN system at $\mathcal{O}(\varepsilon^2)$. These diagrams are classified as the football diagram ($F_{1.1}$), triangle diagrams ($T_{1.i}$), box diagrams ($B_{1.i}$), and crossed box diagrams ($R_{1.i}$). We use the heavy-thick line to denote the $\Delta(1232)$ in the loops. Other notations are the same as those in Fig. 1.

$$\mathcal{V}_{DN}^{T_{1.3}} = (\mathbf{I}_1\cdot\mathbf{I}_2)\frac{g_a^2}{f_\pi^4}\left[(d-1)J_{34}^T - \boldsymbol{q}^2(J_{24}^T + J_{33}^T)\right](m_\pi,\mathcal{E},q), \tag{17}$$

$$\begin{aligned}\mathcal{V}_{DN}^{B_{1.1}} = &\left[\frac{1}{8}-\frac{1}{3}\mathbf{I}_1\cdot\mathbf{I}_2\right]\frac{3g^2g_a^2}{2f_\pi^4}\Big[\boldsymbol{q}^4(J_{22}^B+2J_{32}^B+J_{43}^B)\\ &+(d^2-1)J_{41}^B-2\boldsymbol{q}^2(d+1)(J_{31}^B+J_{42}^B)\\ &-\boldsymbol{q}^2J_{21}^B\Big](m_\pi,\mathcal{E},\mathcal{E}-\delta_b,q),\end{aligned} \tag{18}$$

$$\begin{aligned}\mathcal{V}_{DN}^{B_{1.2}} = &\left[\frac{1}{2}+\frac{2}{3}\mathbf{I}_1\cdot\mathbf{I}_2\right]\frac{g^2g_\delta^2}{f_\pi^4}\Big[\boldsymbol{q}^4\frac{d-2}{d-1}(J_{22}^B+2J_{32}^B+J_{43}^B)\\ &+(d^2-d-2)J_{41}^B-2\boldsymbol{q}^2\frac{d^2-d-2}{d-1}(J_{31}^B+J_{42}^B)\\ &-\boldsymbol{q}^2\frac{d-2}{d-1}J_{21}^B\Big](m_\pi,\mathcal{E}-\delta_a,\mathcal{E}-\delta_b,q),\end{aligned} \tag{19}$$

where the loop functions J_{ij}^F, J_{ij}^T, J_{ij}^B, and J_{ij}^R are defined and given in Refs. [64–66]. d is the dimension introduced in the dimensional regularization. $\mathcal{E}=E_i-m_i[i=N,D^{(*)}]$ represents the residual energies of the N and $D^{(*)}$. $\mathcal{E}$ is set to zero in our calculations. The expressions of the crossed box diagrams $(R_{1.i})$ can be obtained with the relation

$$\mathcal{V}_{DN}^{R_{1.i}} = \mathcal{V}_{DN}^{B_{1.i}}\Big|_{J_{ij}^B\to J_{ij}^R,\mathbf{I}_1\cdot\mathbf{I}_2\to-\mathbf{I}_1\cdot\mathbf{I}_2}. \tag{20}$$

In order to generate the effective potential, one needs to subtract the two particle reducible contributions from the box diagrams. A detailed deduction that based on the principal value integral method is given in the Appendix B of Ref. [66].

The $\mathcal{O}(\varepsilon^2)$ two-pion-exchange diagrams for the D^*N system are shown in Fig. 3. Their analytical expressions are written as

$$\mathcal{V}_{D^*N}^{F_{2.1}} = (\mathbf{I}_1\cdot\mathbf{I}_2)\frac{1}{f_\pi^4}J_{22}^F(m_\pi,q), \tag{21}$$

$$\mathcal{V}_{D^*N}^{T_{2.1}} = (\mathbf{I}_1\cdot\mathbf{I}_2)\frac{g^2}{f_\pi^4}\left[2J_{34}^T-\boldsymbol{q}^2\frac{d-2}{d-1}(J_{24}^T+J_{33}^T)\right](m_\pi,\mathcal{E},q), \tag{22}$$

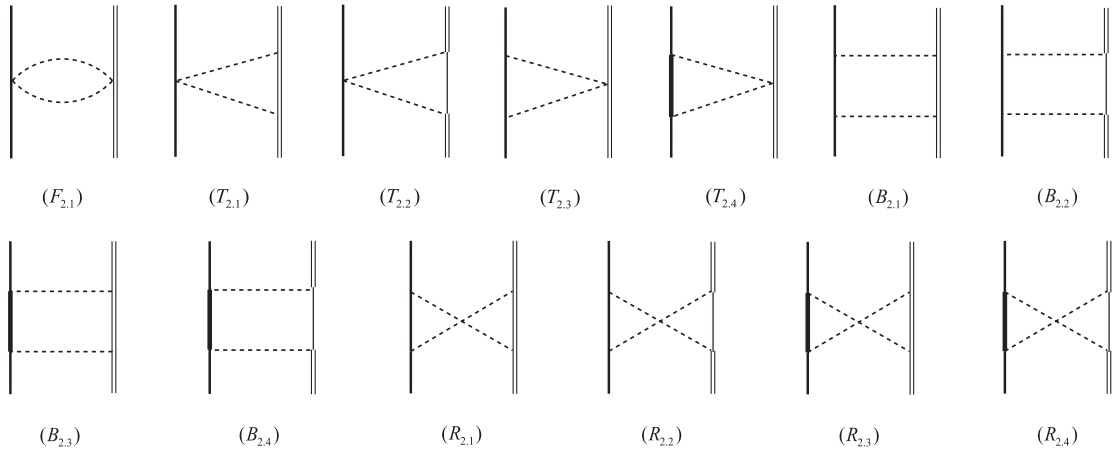

FIG. 3. The two-pion-exchange diagrams of the D^*N system at $\mathcal{O}(\varepsilon^2)$. The notations are the same as those in Fig. 2.

$$\mathcal{V}^{T_{2.2}}_{D^*N} = (\mathbf{I}_1\cdot\mathbf{I}_2)\frac{g^2}{f_\pi^4}\left[J^T_{34}-\frac{\boldsymbol{q}^2}{d-1}(J^T_{24}+J^T_{33})\right](m_\pi,\mathcal{E}+\delta_b,q), \tag{23}$$

$$\mathcal{V}^{T_{2.3}}_{D^*N} = (\mathbf{I}_1\cdot\mathbf{I}_2)\frac{g_a^2}{f_\pi^4}\left[(d-1)J^T_{34}-\boldsymbol{q}^2(J^T_{24}+J^T_{33})\right](m_\pi,\mathcal{E},q), \tag{24}$$

$$\mathcal{V}^{T_{2.4}}_{D^*N} = (\mathbf{I}_1\cdot\mathbf{I}_2)\frac{4g_\delta^2}{3f_\pi^4}\left[(2-d)J^T_{34}-\boldsymbol{q}^2\frac{2-d}{d-1}(J^T_{24}+J^T_{33})\right](m_\pi,\mathcal{E}-\delta_a,q), \tag{25}$$

$$\begin{aligned}\mathcal{V}^{B_{2.1}}_{D^*N} = &\left[\frac{1}{8}-\frac{1}{3}\mathbf{I}_1\cdot\mathbf{I}_2\right]\frac{3g^2g_a^2}{2f_\pi^4}\left[\frac{4d^2-10d+6}{d-1}J^B_{41}-\boldsymbol{q}^2\frac{d^2+3d-8}{d-1}(J^B_{31}+J^B_{42})\right.\\&\left.-\boldsymbol{q}^2\frac{d-2+\boldsymbol{\sigma}\cdot\boldsymbol{T}}{d-1}J^B_{21}+\boldsymbol{q}^4\frac{d-2}{d-1}(J^B_{22}+2J^B_{32}+J^B_{43})\right](m_\pi,\mathcal{E},\mathcal{E},q),\end{aligned} \tag{26}$$

$$\begin{aligned}\mathcal{V}^{B_{2.2}}_{D^*N} = &\left[\frac{1}{8}-\frac{1}{3}\mathbf{I}_1\cdot\mathbf{I}_2\right]\frac{3g^2g_a^2}{2f_\pi^4}\left[-2\boldsymbol{q}^2\frac{d+1}{d-1}(J^B_{31}+J^B_{42})-\boldsymbol{q}^2\frac{1}{d-1}(1+\boldsymbol{\sigma}\cdot\boldsymbol{T})J^B_{21}\right.\\&\left.+(d+1)J^B_{41}+\boldsymbol{q}^4\frac{1}{d-1}(J^B_{22}+2J^B_{32}+J^B_{43})\right](m_\pi,\mathcal{E},\mathcal{E}+\delta_b,q),\end{aligned} \tag{27}$$

$$\begin{aligned}\mathcal{V}^{B_{2.3}}_{D^*N} = &\left[\frac{1}{2}+\frac{2}{3}\mathbf{I}_1\cdot\mathbf{I}_2\right]\frac{g^2g_\delta^2}{f_\pi^4}\left[-\boldsymbol{q}^2\frac{(d-2)^2-\boldsymbol{\sigma}\cdot\boldsymbol{T}}{(d-1)^2}J^B_{21}-\boldsymbol{q}^2\frac{(d-2)(d^2+3d-8)}{(d-1)^2}(J^B_{31}+J^B_{42})\right.\\&\left.+\frac{2(d^2-2d+2)}{d-1}J^B_{41}+\boldsymbol{q}^4\frac{(d-2)^2}{(d-1)^2}(J^B_{22}+2J^B_{32}+J^B_{43})\right](m_\pi,\mathcal{E}-\delta_a,\mathcal{E},q),\end{aligned} \tag{28}$$

$$\begin{aligned}\mathcal{V}^{B_{2.4}}_{D^*N} = &\left[\frac{1}{2}+\frac{2}{3}\mathbf{I}_1\cdot\mathbf{I}_2\right]\frac{g^2g_\delta^2}{f_\pi^4}\frac{1}{d-1}\left[-2\boldsymbol{q}^2\frac{(d+1)(d-2)}{d-1}(J^B_{31}+J^B_{42})-\boldsymbol{q}^2\frac{d-2-\boldsymbol{\sigma}\cdot\boldsymbol{T}}{d-1}J^B_{21}\right.\\&\left.+\boldsymbol{q}^4\frac{d-2}{d-1}(J^B_{22}+2J^B_{32}+J^B_{43})+(d^2-d-2)J^B_{41}\right](m_\pi,\mathcal{E}-\delta_a,\mathcal{E}+\delta_b,q).\end{aligned} \tag{29}$$

The expressions of the diagrams $(R_{2.i})$ can be obtained with

$$\mathcal{V}^{R_{2.i}}_{D^*N} = \mathcal{V}^{B_{2.i}}_{D^*N}|_{J^B_x\to J^R_x,\mathbf{I}_1\cdot\mathbf{I}_2\to-\mathbf{I}_1\cdot\mathbf{I}_2,\boldsymbol{\sigma}\cdot\boldsymbol{T}\to-\boldsymbol{\sigma}\cdot\boldsymbol{T}}. \tag{30}$$

In the above equations, the spin operator and transferred momentum are defined in d dimensions, such as $\boldsymbol{S}^2 = (d-1)/4$ [69] and $q_iq_j = 1/(d-1)\boldsymbol{q}^2\delta_{ij}$ for the S wave. The relation between the $\boldsymbol{T}$ operator and the polarization vector of D^* meson can be found in Appendix C of Ref. [66].

Notably, because of $\delta_b > m_\pi$, some diagrams in Fig. 3, such as $(T_{2.2})$ and $(B_{2.2})$, would also generate imaginary parts, which contribute to the width of the corresponding bound state. If solving the Lippmann-Schwinger equation, the imaginary part would shift the pole position in the Riemann sheet. In this work, we solve the Schrödinger equation to only focus on the binding energies; thus, the imaginary parts are ignored in our calculations.

At the next-to-leading order, besides the two-pion-exchange potentials illustrated above, we also have the one-loop corrections to the one-pion-exchange and contact terms. These corrections can be replaced by using the physical values of the couplings, decay constant, and masses of pion, N and D mesons, etc. In addition, the subleading contact Lagrangians are also necessary. On the one hand, they are responsible for the renormalizations of two-pion-exchange loop diagrams. Because these diagrams are usually ultraviolet divergent in $d = 4$ dimensions, we need the unrenormalized $\mathcal{O}(\varepsilon^2)$ LECs to absorb the divergent parts of the loop functions in Eqs. (14)–(29). On the other hand, these $\mathcal{O}(\varepsilon^2)$ Lagrangians may generate contact interactions with two powers of momenta in the following form [58]:

$$\begin{aligned}\mathscr{V} = &C_1\boldsymbol{q}^2+C_2\boldsymbol{k}^2+(C_3\boldsymbol{q}^2+C_4\boldsymbol{k}^2)\boldsymbol{\sigma}\cdot\boldsymbol{T}\\&+C_5[i\boldsymbol{S}\cdot(\boldsymbol{q}\times\boldsymbol{k})]+C_6(\boldsymbol{\sigma}\cdot\boldsymbol{q})(\boldsymbol{T}\cdot\boldsymbol{q})\\&+C_7(\boldsymbol{\sigma}\cdot\boldsymbol{k})(\boldsymbol{T}\cdot\boldsymbol{k}),\end{aligned} \tag{31}$$

where $\boldsymbol{k}=(\boldsymbol{p}_N+\boldsymbol{p}_D)/2$ is the average momentum and $\boldsymbol{S}=(\boldsymbol{S}_N+\boldsymbol{S}_{D^*})/2$ is the total spin. (Note that for the DN system, only the C_1, C_2, and C_5 terms survive.) Unlike the NN case, these $\mathcal{O}(\varepsilon^2)$ LECs cannot be fitted at present since the $D^{(*)}N$ scattering data is still unavailable. So we ignore their contributions and only consider the leading order contact terms. Once the $D^{(*)}N$ scattering phase shifts in lattice QCD simulations are available, it would be an intriguing topic to restudy this system while considering higher order contributions.

III. NUMERICAL RESULTS AND DISCUSSIONS

With the momentum-space potentials $\mathcal{V}(\boldsymbol{q})$ obtained in Sec. II B, we make the following Fourier transformation to get the effective potential $V(r)$ in the coordinate space,

$$V(r)=\int\frac{d^3\boldsymbol{q}}{(2\pi)^3}e^{i\boldsymbol{q}\cdot\boldsymbol{r}}\mathcal{V}(\boldsymbol{q})\mathcal{F}(\boldsymbol{q}). \tag{32}$$

We need to introduce a regulator $\mathcal{F}(\boldsymbol{q})$ to suppress the high momentum contribution. We choose the Gauss form $\mathcal{F}(\boldsymbol{q})=\exp(-\boldsymbol{q}^{2n}/\Lambda^{2n})$ as used in the NN and $N\bar{N}$ systems [77,78]. The Taylor expansion of the regulator function gives $\mathcal{F}(\boldsymbol{q})=1-\boldsymbol{q}^{2n}/\Lambda^{2n}+\cdots$. The power n is chosen to be sufficiently large in order that the cutoff induced contributions $\mathcal{V}(\boldsymbol{q})\mathcal{O}(\boldsymbol{q}^{2n}/\Lambda^{2n})$ are beyond the chiral order one is working at. In our calculation, we only consider the leading and subleading contributions, thus $n=1$ is already enough in our case. However, we use the $N\bar{N}$ LECs fitted in Ref. [79] to estimate the LECs of $D^{(*)}N$ systems, where the $n=3$ is adopted in Ref. [79], so we also choose $n=3$ for consistency. The power $n=3$ and cutoff $\Lambda\simeq 0.5\pm 0.1$ GeV are always adopted to fit the experimental data and make predictions [79,80,80–82].

A. Numerical results

In order to get the numerical results, we also need to know the values of the four LECs in Eq. (9). Generally, these LECs should be determined by fitting the $D^{(*)}N$ scattering data in experiments or in lattice QCD simulations. However, the data in this area are scarce; thus, we have to resort to other alternative ways. As proposed in Refs. [67,68], we estimate the LECs by constructing the contact Lagrangian at the quark level, and then extract the couplings from the $N\bar{N}$ interaction, which is demonstrated in the Appendix.

We show the effective potentials of each possible $I(J^P)$ configuration in Fig. 4. In the following, we analyze the behaviors of effective potentials for each system.

DN system: The result in Fig. 4(a) shows that the $\mathcal{O}(\varepsilon^0)$ contact and $\mathcal{O}(\varepsilon^2)$ two-pion-exchange potentials of the $[DN]^{I=0}_{J=1/2}$ system are both attractive. But the attraction of two-pion-exchange potential is rather weak. The attractive potential is dominantly provided by the contact interaction. We find a bound state in this channel. The binding energy and mass of this state are predicted, respectively,

$$\begin{aligned}\Delta E_{[DN]^{I=0}_{J=1/2}}&\simeq -11.1\ \text{MeV},\\ M_{[DN]^{I=0}_{J=1/2}}&\simeq 2792.0\ \text{MeV}.\end{aligned} \tag{33}$$

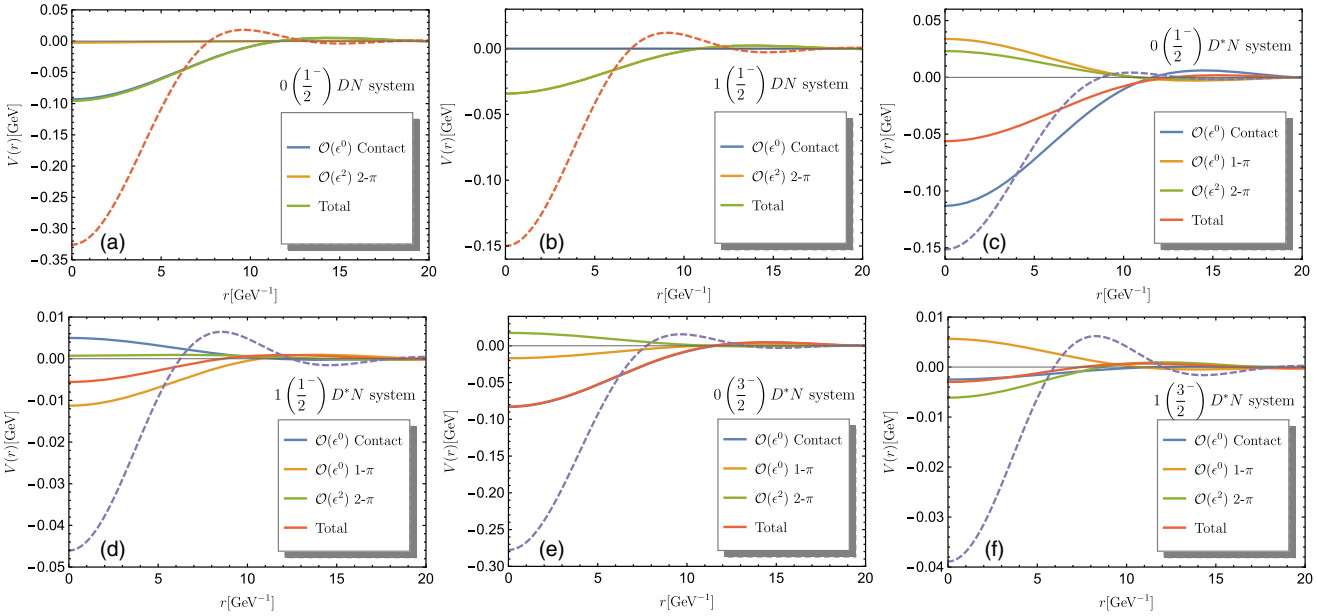

FIG. 4. The effective potentials of the $D^{(*)}N$ systems. Their $I(J^P)$ are marked in each subfigure. The potentials with the solid lines are obtained with the cutoff parameter $\Lambda=0.4$ GeV and the LECs estimated in the Appendix. The corresponding total potentials with the dashed lines are obtained with the cutoff parameter $\Lambda=0.6$ GeV.

For the $[DN]^{I=1}_{J=1/2}$ system in Fig. 4(b), the $\mathcal{O}(\varepsilon^0)$ contact interaction vanishes in our calculation, and the total potential arises from the two-pion-exchange contribution. We notice the potential in this channel is much shallower than that of the $[DN]^{I=0}_{J=1/2}$ channel, i.e., the attraction is too feeble to form the bound state. Thus the binding solution does not exist in this channel.

D^*N system: The contact potential of the $[D^*N]^{I=0}_{J=1/2}$ system in Fig. 4(c) is attractive, while the one-pion-exchange and two-pion-exchange interactions are both repulsive. Therefore, the total potential is shallower than that of the $[DN]^{I=0}_{J=1/2}$ channel. However, we still obtain a binding solution in the $[D^*N]^{I=0}_{J=1/2}$ system. The binding energy and mass of this state are

$$\Delta E_{[D^*N]^{I=0}_{J=1/2}} \simeq -1.5 \text{ MeV},$$
$$M_{[D^*N]^{I=0}_{J=1/2}} \simeq 2943.6 \text{ MeV}. \quad (34)$$

For the $[D^*N]^{I=1}_{J=1/2}$ system in Fig. 4(d), the one-pion-exchange potential is weakly attractive, but the contact and two-pion-exchange potentials are all repulsive. Thus, the total attractive potential is not strong enough to form molecular states in this channel.

For the channel $[D^*N]^{I=0}_{J=3/2}$ in Fig. 4(e), the behavior of its potentials is very interesting. We notice the one-pion- and two-pion-exchange contributions almost cancel each other. Thus, the total potential is mainly provided by the contact term, which can reach up to -80 MeV at the deepest position. By solving the Schrödinger equation, we find the binding solution in the $[D^*N]^{I=0}_{J=3/2}$ system, and the binding energy is

$$\Delta E_{[D^*N]^{I=0}_{J=3/2}} \simeq -6.7 \text{ MeV}. \quad (35)$$

The corresponding mass of this bound state is

$$M_{[D^*N]^{I=0}_{J=3/2}} \simeq 2938.4 \text{ MeV}, \quad (36)$$

which is in good agreement with the mass of $\Lambda_c(2940)$ measured by *BABAR*, Belle, and LHCb (e.g., see Table I).

For the last channel $[D^*N]^{I=1}_{J=3/2}$ in Fig. 4(f), the one-pion- and two-pion-exchange potentials almost cancel each other and the contact contribution is very weakly attractive. Thus, no bound state can be found in this channel.

Role of the $\Delta(1232)$: Considering the strong coupling between $\Delta(1232)$ and $N\pi$, we include the contribution of $\Delta(1232)$ in the loop diagrams (e.g., see Figs. 2 and 3). Here, we discuss the role of $\Delta(1232)$ in the effective potentials of the DN and D^*N systems. We try to ignore the effect of $\Delta(1232)$, and notice that the line shape of the two-pion-exchange potentials changes drastically. Except for the $[DN]^{I=1}_{J=1/2}$, the whole behavior of the other channels is totally reversed. For example, the two-pion-exchange potential of the $[DN]^{I=0}_{J=1/2}$ channel becomes repulsive, which renders the total potential of this channel shallower. But for the $[D^*N]^{I=0}_{J=3/2}$ channel, the two-pion-exchange potential becomes attractive. The variation is about -30 MeV, which gives rise to a deeper attractive potential, and the binding energy is -16 MeV.

In general, the conclusion that there exists the bound state in the isoscalar $[D^{(*)}N]_J$ channel and no binding solution in the isovector channel is robust, whether we consider the $\Delta(1232)$ or not. However, the $\Delta(1232)$ plays an important role in determining the physical masses of $\Lambda_c(2940)$ and other bound states, since the molecular states are very sensitive to the subtle changes of their internal effective potentials.

It is also interesting to see the dependence of the potentials on cutoff Λ. The results for $\Lambda = 0.6$ GeV are shown as the dashed lines in Fig. 4. We notice the change is dramatic, the total potentials are sensitive to the cutoff, and they all become much deeper when the cutoff is varied to 0.6 GeV. The binding energies for $[DN]^{I=0}_{J=1/2}$, $[D^*N]^{I=0}_{J=1/2}$, and $[D^*N]^{I=0}_{J=3/2}$ channels in this case are -76.7, -11.6, and -55.1 MeV, respectively. The isovector DN system also starts to form a bound state with binding energy -1.0 MeV, but we still cannot get binding solutions in the isovector D^*N system. Of course, this behavior is foreseeable because we introduced a Gaussian regulator when making the Fourier transformation [see Eq. (32)]. Even in the NN interactions, the LECs show mild dependence on the cutoff over a narrow range only when the higher order contributions are included [83,84]. Generally, the LECs are used to absorb the scale dependence of observables when making the nonperturbative renormalizations; i.e., they are usually the functions of cutoff Λ. Therefore, varying the cutoff with the fixed LECs might be unreasonable. In the Appendix, we illustrate the results with the LECs fixed at $\Lambda = 0.6$ GeV from Ref. [79].

Inspecting the potentials in Fig. 4 one can find two defects, one is the one-pion-exchange potential does not have a longer range than the two-pion exchange one and even the contact interaction, another one is where a bump appeared in the total potentials. Both are caused by the artificial effect from the Gaussian regulator. As indicated in Refs. [80,85], such a form regulator would distort the partial waves and affect the long-range parts of the interactions. If the cutoff is sufficiently large, the induced artifacts are expected to go beyond the accuracy at the order we are conducting. However, they may become an issue when the cutoff resides in the low scale. Additionally, the $\mathcal{F}(\boldsymbol{q})$ in Eq. (32) has the risk of mixing different partial waves. But for the S wave, the mixing effect is insufficient to impact the main feature of the potentials.

B. Discussions

No binding solution in the isovector channel indicates that the $[DN]^{I=1}_{J=1/2}$ molecular explanation of $\Sigma_c(2800)$ is

not favored. Although the $\Sigma_c(2800)$ is near the DN threshold, its mass is also consistent with the quark model predictions [14,42,43,86,87]. Thus, interpreting the $\Sigma_c(2800)$ as the $1P$ charmed baryon seems to be more reasonable.

The situation of $\Lambda_c(2940)$ is very similar to the $\Lambda(1405)$, $D_{s0}(2317)$, and $X(3872)$; i.e., there is large gap between the physical states and quark model predictions.[2] Generally, one possible reason is these states *per se* may be exotic rather than conventional.

A recent analysis from LHCb gives weak constraints on the J^P quantum numbers of $\Lambda_c(2940)$, where $J^P = \frac{3}{2}^-$ is favored [12]. This is consistent with our calculations. Actually, one can notice two peaks in the D^0p invariant mass spectrum from 2.92 to 2.99 GeV in the results of LHCb [see Fig. 13(a) in Ref. [12]]. The one at 2.94 GeV is just the reported $\Lambda_c(2940)$. The other peak at 2.98 GeV may correspond to the true $\Lambda_c(2P)$ baryon, since its mass is close to the quark model prediction [13–16]. Our calculation indicates the $\Lambda_c(2940)$ is probably the S-wave D^*N molecular state.

We report three bound states in the $[DN]^{I=0}_{J=1/2}$, $[D^*N]^{I=0}_{J=1/2}$, and $[D^*N]^{I=0}_{J=3/2}$ systems. They are very similar to the newly observed $P_c(4312)$, $P_c(4440)$, and $P_c(4457)$ at LHCb [89], which are interpreted as the $[\bar{D}\Sigma_c]^{I=1/2}_{J=1/2}$, $[\bar{D}^*\Sigma_c]^{I=1/2}_{J=1/2}$, and $[\bar{D}^*\Sigma_c]^{I=1/2}_{J=3/2}$ molecular states [65,66], respectively. If $\Lambda_c(2940)$ is indeed the D^*N molecular states, then it should contain two structures, i.e., $[D^*N]^{I=0}_{J=1/2}$ and $[D^*N]^{I=0}_{J=3/2}$. Because the mass splitting between the spin-$\frac{1}{2}$ and spin-$\frac{3}{2}$ states is only about 5 MeV, it is very difficult to disassemble these two structures with current accuracy. A similar situation has happened to the P_c states. The previously reported $P_c(4450)$ [90] contains two structures, $P_c(4440)$ and $P_c(4457)$, after increasing the data sample. More interesting, we find the mass of the spin-$\frac{1}{2}$ state is larger than that of the spin-$\frac{3}{2}$ one.

The signal of $\Lambda_c(2940)$ has been observed in the D^0p and $\Sigma_c\pi$ final states [10–12]. However, if the J^P of $\Lambda_c(2940)$ is $\frac{3}{2}^-$ as weakly constrained by the LHCb, then it decays into the D^0p and $\Sigma_c\pi$ through the D-wave, which is strongly suppressed.[3] Therefore, as mentioned above, one promising explanation is that the $\Lambda_c(2940)$ signal actually contains two structures. The spin-$\frac{1}{2}$ structure can easily decay into D^0p and $\Sigma_c\pi$ via the S wave.

[2]An unquenched study with the channel coupling in Ref. [88] declares the mass of $\Lambda_c(2P, 3/2^-)$ state can be lowered down to match the experimental data of $\Lambda_c(2940)$.

[3]Based on the $^3P_0$ model calculation, the large decay width of $\Lambda_c(2940) \to D^0p$ is reported in Refs. [91,92] by treating $\Lambda_c(2940)$ as a $2P$ state in the Λ_c family, but the low mass puzzle still exist.

TABLE II. The predicted binding energies and masses for the isoscalar $[D^{(*)}N]_J$ and $[\bar{B}^{(*)}N]_J$ systems (in units of MeV).

System	$[DN]_{\frac{1}{2}}$	$[D^*N]_{\frac{1}{2}}$	$[D^*N]_{\frac{3}{2}}$	$[\bar{B}N]_{\frac{1}{2}}$	$[\bar{B}^*N]_{\frac{1}{2}}$	$[\bar{B}^*N]_{\frac{3}{2}}$
ΔE	−11.1	−1.5	−6.7	−8.8	−3.5	−8.4
Mass	2792.0	2943.6	2938.4	6208.8	6259.4	6254.5

Borrowing experiences from the discovery of P_c states, we urge the experimenters to reanalyze the $\Lambda_c^+\pi^+\pi^-$ invariant mass spectrum with the accumulated data, since the $[DN]^{I=0}_{J=1/2}$, $[D^*N]^{I=0}_{J=1/2}$, and $[D^*N]^{I=0}_{J=3/2}$ bound states can all decay into $\Sigma_c^0\pi^+$.

In addition to the mass spectrum, the decay pattern can also give us some important criteria to identify the inner structure of $\Lambda_c(2940)$. In the molecular scenario, the D^*N system can easily decay into the DN channel via the pion exchange, while the $\Sigma_c\pi$ decay mode requires the exchange of a nucleon or a D meson. Thus, the decay amplitude of the D^0p mode should be much larger than that of the $\Sigma_c\pi$, because the heavy hadron exchange is generally suppressed. However, the phase space of the $\Sigma_c\pi$ mode is larger.

The three body decay mode is also very interesting. We take the decay modes of the $X(3872)$ and other higher charmonia as an example. The branching fraction of $X(3872) \to D^0\bar{D}^0\pi^0$ can reach up to 40% [1]. In contrast, the open charm three body decays of the higher charmonia are only a few percents [93]. Analogously, the branching fraction of $\Lambda_c(2940) \to D^0\pi^0(\gamma)p$ should also be conspicuous in the molecular picture.

Besides, our study can be easily extended to the $\bar{B}^{(*)}N$ systems. The axial coupling g and mass splitting δ_b in Eq. (7) should be replaced by the bottomed ones, where we adopt $g = -0.52$ [94,95] and $\delta_b = 45$ MeV [1]. The predicted results are listed in Table. II. There also exist bound states in the isoscalar $[\bar{B}^{(*)}N]_J$ systems. These states might be reconstructed at the $\Lambda_b^0\pi^+\pi^-$ final states, and the $[\bar{B}^*N]_J$ states could also be detected in the B^-p mass spectrum.

IV. SUMMARY

A sophisticated investigation on the DN and D^*N interactions is crucial to clarify the nature of the charmed baryons $\Sigma_c(2800)$ and $\Lambda_c(2940)$. In this work, we systematically study the effective potentials of the DN and D^*N systems with the chiral effective field theory up to the next-to-leading order. We simultaneously consider the contributions of the long-range one-pion-exchange, mid-range two-pion-exchange, and short-range contact term. We also include the $\Delta(1232)$ as an intermediate state in the loop diagrams. The LECs are estimated from the $N\bar{N}$ interaction with the help of the quark model.

For the DN system, our calculation shows the effective potentials of the $[DN]^{I=0}_{J=1/2}$ and $[DN]^{I=1}_{J=1/2}$ channels are both attractive. We find a bound state in the $[DN]^{I=0}_{J=1/2}$ channel, but the attraction in the $[DN]^{I=1}_{J=1/2}$ channel is too weak to form a bound state. Thus, the explanation of $\Sigma_c(2800)$ as the DN molecular state is disfavored in our calculations. The $\Sigma_c(2800)$ is more likely to be the conventional $1P$ charmed baryon, since its mass is well consistent with the quark model prediction.

There are four channels in the $[D^*N]^I_J$ system. We find only the isoscalar $[D^*N]_J$ potential is deep enough to form the molecular state. We obtain the masses of the bound states in the $[D^*N]^{I=0}_{J=1/2}$ and $[D^*N]^{I=0}_{J=3/2}$ channels to be 2943.6 and 2938.4 MeV, respectively, which well accord with the *BABAR*, Belle, and LHCb measurements for $\Lambda_c(2940)$. Considering the small mass splitting between the spin-$\frac{1}{2}$ and spin-$\frac{3}{2}$ states, we conjecture the $\Lambda_c(2940)$ signal contains two structures.

It is not so easy to squeeze the $\Lambda_c(2940)$ into the conventional charmed baryon spectrum, since the 60–100 MeV gap between the physical mass and quark model prediction cannot be readily remedied. However, this problem can be easily reconciled in the molecular picture; i.e., the $\Lambda_c(2940)$ is probably the isoscalar D^*N molecule rather than the $2P$ charmed baryon.

We also investigate the influence of $\Delta(1232)$ in the loop diagrams. The binding solutions always exist in the isoscalar $[D^*N]_J$ channels no matter if we include the $\Delta(1232)$ or not. There still do not exist bound states in the isovector channels even when we ignore the $\Delta(1232)$. However, the $\Delta(1232)$ is important in yielding the shallowly bound isoscalar $[D^{(*)}N]_J$ states.

We hope experimentalists could seek for the pentaquark candidates in the open charmed channels, where the $D^{(*)}N$ molecular pentaquarks in the isoscalar systems might be reconstructed at the $\Lambda_c^+\pi^+\pi^-$ final state.

ACKNOWLEDGMENTS

B. W. is very grateful to X. Z. Weng for discussions on the charmed baryon spectroscopy. This project is supported by the National Natural Science Foundation of China under Grant No. 11975033.

APPENDIX: DETERMINING THE LECs FROM $N\bar{N}$ INTERACTION

One needs to know the values of the LECs in Eq. (9) to study the strength of the short-range interaction. As proposed in Refs. [67,68] (more details can be found in the Appendix of these two references), the LECs of $D^{(*)}N$ systems can be bridged to those of the $N\bar{N}$ interaction with the help of quark model. The way is analogous to the resonance saturation model [96], but we build the quark level Lagrangian. We assume the contact interaction stems from the heavy meson exchanging. We introduce $\mathcal{S}$ and $\mathcal{A}^\mu$ to produce the central potential and spin-spin interaction, respectively. The matrix form of $\mathcal{S}$ and $\mathcal{A}^\mu$ can be expressed as

TABLE III. The matrix elements of the operator $\sum_{i\in h_a, j\in h_b}\mathcal{O}_{ij}$, where h_a and h_b are two hadrons. $\mathcal{O}_{ij}$ is the two-body interaction operator between quarks.

$\mathcal{O}_{ij}$	$\mathbf{1}_{ij}$	$\boldsymbol{\tau}_i\cdot\boldsymbol{\tau}_j$	$\boldsymbol{\sigma}_i\cdot\boldsymbol{\sigma}_j$	$(\boldsymbol{\tau}_i\cdot\boldsymbol{\tau}_j)(\boldsymbol{\sigma}_i\cdot\boldsymbol{\sigma}_j)$
$[N\bar{N}]^{I=1}_{J=0}$	9	1	−3	$-\frac{25}{3}$
$[D^*N]^{I=1}_{J=3/2}$	3	1	1	$\frac{5}{3}$

$$\mathcal{S} = \mathcal{S}_3^i\tau^i + \sqrt{\frac{1}{3}}\mathcal{S}_1, \tag{A1}$$

$$\mathcal{A}^\mu = \mathcal{A}_3^{\mu i}\tau^i + \sqrt{\frac{1}{3}}\mathcal{A}_1^\mu, \tag{A2}$$

where $\mathcal{S}_3$ ($\mathcal{A}_3^\mu$) and $\mathcal{S}_1$ ($\mathcal{A}_1$) denote the isospin triplet and isospin singlet, respectively. The coefficient $\sqrt{\frac{1}{3}}$ is introduced to satisfy the SU(3) flavor symmetry.

The $q\bar{q}$ contact potential can be written as

$$V_{q\bar{q}} = c_s(1-3\boldsymbol{\tau}_1\cdot\boldsymbol{\tau}_2) + c_t(1-3\boldsymbol{\tau}_1\cdot\boldsymbol{\tau}_2)\boldsymbol{\sigma}_1\cdot\boldsymbol{\sigma}_2, \tag{A3}$$

where c_s and c_t are the coupling constants. The minus sign in Eq. (A3) arises since the isospin triplet and the isospin singlet have the different G parities.

With the $q\bar{q}$ contact potential $V_{q\bar{q}}$ in Eq. (A3) and the relevant matrix element in Table III, we obtain the $N\bar{N}$ contact potential as follows:

$$\begin{aligned} V_{N\bar{N}} &= \langle N\bar{N}|V_{q\bar{q}}|N\bar{N}\rangle = 9c_s - 3c_s\boldsymbol{\tau}_1\cdot\boldsymbol{\tau}_2 \\ &\quad + c_t\boldsymbol{\sigma}_1\cdot\boldsymbol{\sigma}_2 - \frac{25}{3}c_t(\boldsymbol{\tau}_1\cdot\boldsymbol{\tau}_2)(\boldsymbol{\sigma}_1\cdot\boldsymbol{\sigma}_2). \end{aligned} \tag{A4}$$

Similarly, the D^*N contact potential can be easily worked out,

$$\begin{aligned} V_{D^*N} &= \langle D^*N|V_{q\bar{q}}|D^*N\rangle = 3c_s - 12c_s\mathbf{I}_1\cdot\mathbf{I}_2 \\ &\quad - c_t\boldsymbol{\sigma}\cdot\mathbf{T} + 20c_t(\mathbf{I}_1\cdot\mathbf{I}_2)(\boldsymbol{\sigma}\cdot\mathbf{T}). \end{aligned} \tag{A5}$$

Matching Eq. (11) and Eq. (A5) one can get the LECs in Eq. (9), which read

$$D_a = 3c_s, \quad D_b = -c_t, \quad E_a = 3c_s, \quad E_b = -5c_t. \tag{A6}$$

Therefore, once we know the values of c_s and c_t, we can capture the short-range interaction of the $D^{(*)}N$ systems. The c_s and c_t can be extracted from the $N\bar{N}$ interaction, and

the $N\bar{N}$ scattering phase shift has been fitted in the framework of chiral effective field theory to the next-to-next-to-leading order in Ref. [79]. Using the values of $\tilde{C}_{^3S_1}$ in the $I=0$ and $I=1$ channels fitted at $(\Lambda,\tilde{\Lambda})=(450,500)$ MeV as inputs, we obtain

$$c_s=-8.1\ \text{GeV}^{-2},\qquad c_t=0.65\ \text{GeV}^{-2}. \tag{A7}$$

We notice $|c_s|/|c_t|\simeq 12.5$, i.e., the spin-spin interaction only serves as a perturbation to give mass splittings between spin multiplets.

In addition, Ref. [79] also gives the fitted results with cutoff combination $(\Lambda,\tilde{\Lambda})=(650,700)$ MeV. With the LECs of $\tilde{C}_{^3S_1}$ in the $I=0$ and $I=1$ channels fitted at $(\Lambda,\tilde{\Lambda})=(650,700)$ MeV as inputs we obtain

$$c_s=-11.1\ \text{GeV}^{-2},\qquad c_t=4.5\ \text{GeV}^{-2}. \tag{A8}$$

We see the c_s value is similar to the one in Eq. (A7), while c_t becomes much larger. (We find that using other channel combinations in Ref. [79] as inputs always obtains the c_s value with the similar size and the same sign, but c_t varies a lot.) With the LECs in Eq. (A8) as inputs we get the binding energies of the isoscalar and isovector $D^{(*)}N$ systems as listed in Table IV. One can notice that the binding energies of the $[DN]^{I=0}_{J=1/2}$ and $[D^*N]^{I=0}_{J=1/2}$ channels are quite large, which can reach up to hundreds of MeV. This is highly unnatural in our framework, so we intend to use the moderate LECs in Eq. (A7) rather than the ones in Eq. (A8) to give predictions. However, we still can capture a gross indication that the isoscalar channel is always bound, while the isovector channel is not (except for the $[DN]^{I=1}_{J=1/2}$ channel).

TABLE IV. The predicted binding energies for the isoscalar and isovector $[D^{(*)}N]_J$ system (in units of MeV) in the case of $c_s=-11.1\ \text{GeV}^{-2}$, $c_t=4.5\ \text{GeV}^{-2}$, and $\Lambda=0.6$ GeV. The "×" denotes no binding solution.

	$I=0$			$I=1$		
System	$[DN]_{\frac{1}{2}}$	$[D^*N]_{\frac{1}{2}}$	$[D^*N]_{\frac{3}{2}}$	$[DN]_{\frac{1}{2}}$	$[D^*N]_{\frac{1}{2}}$	$[D^*N]_{\frac{3}{2}}$
ΔE	−142.3	−294.8	−19.2	−1.0	×	×

[1] M. Tanabashi *et al.* (Particle Data Group), Review of particle physics, Phys. Rev. D **98**, 030001 (2018).
[2] S. K. Choi *et al.* (Belle Collaboration), Observation of a Narrow Charmonium-Like State in Exclusive $B^{\pm}\to K^{\pm}\pi^{+}\pi^{-}J/\psi$ Decays, Phys. Rev. Lett. **91**, 262001 (2003).
[3] B. Aubert *et al.* (*BABAR* Collaboration), Observation of a Narrow Meson Decaying to $D_s^{+}\pi^0$ at a Mass of 2.32 GeV/c^2, Phys. Rev. Lett. **90**, 242001 (2003).
[4] H. X. Chen, W. Chen, X. Liu, and S. L. Zhu, The hidden-charm pentaquark and tetraquark states, Phys. Rep. **639**, 1 (2016).
[5] F. K. Guo, C. Hanhart, U. G. Meißner, Q. Wang, Q. Zhao, and B. S. Zou, Hadronic molecules, Rev. Mod. Phys. **90**, 015004 (2018).
[6] Y. R. Liu, H. X. Chen, W. Chen, X. Liu, and S. L. Zhu, Pentaquark and tetraquark states, Prog. Part. Nucl. Phys. **107**, 237 (2019).
[7] R. F. Lebed, R. E. Mitchell, and E. S. Swanson, Heavy-quark QCD exotica, Prog. Part. Nucl. Phys. **93**, 143 (2017).
[8] A. Esposito, A. Pilloni, and A. D. Polosa, Multiquark resonances, Phys. Rep. **668**, 1 (2017).
[9] N. Brambilla, S. Eidelman, C. Hanhart, A. Nefediev, C. P. Shen, C. E. Thomas, A. Vairo, and C. Z. Yuan, The *XYZ* states: Experimental and theoretical status and perspectives, arXiv:1907.07583.
[10] B. Aubert *et al.* (*BABAR* Collaboration), Observation of a Charmed Baryon Decaying to D^0p at a Mass Near 2.94 GeV/c^2, Phys. Rev. Lett. **98**, 012001 (2007).
[11] R. Mizuk *et al.* (Belle Collaboration), Experimental Constraints on the Spin and Parity of the $\Lambda_c(2880)^+$, Phys. Rev. Lett. **98**, 262001 (2007).
[12] R. Aaij *et al.* (LHCb Collaboration), Study of the D^0p amplitude in $\Lambda_b^0\to D^0p\pi^-$ decays, J. High Energy Phys. 05 (2017) 030.
[13] S. Capstick and N. Isgur, Baryons in a relativized quark model with chromodynamics, Phys. Rev. D **34**, 2809 (1986).
[14] D. Ebert, R. N. Faustov, and V. O. Galkin, Spectroscopy and Regge trajectories of heavy baryons in the relativistic quark-diquark picture, Phys. Rev. D **84**, 014025 (2011).
[15] B. Chen, K. W. Wei, and A. Zhang, Assignments of Λ_Q and Ξ_Q baryons in the heavy quark-light diquark picture, Eur. Phys. J. A **51**, 82 (2015).
[16] Q. F. Lü, Y. Dong, X. Liu, and T. Matsuki, Puzzle of the Λ_c spectrum, Nucl. Phys. Rev. **35**, 1 (2018).
[17] X. G. He, X. Q. Li, X. Liu, and X. Q. Zeng, $\Lambda_c(2940)^+$: A possible molecular state? Eur. Phys. J. C **51**, 883 (2007).
[18] J. He, Y. T. Ye, Z. F. Sun, and X. Liu, The observed charmed hadron $\Lambda_c(2940)^+$ and the D^*N interaction, Phys. Rev. D **82**, 114029 (2010).
[19] P. G. Ortega, D. R. Entem, and F. Fernandez, Quark model description of the $\Lambda_c(2940)^+$ as a molecular D^*N state and the possible existence of the $\Lambda_b(6248)$, Phys. Lett. B **718**, 1381 (2013).
[20] Y. Dong, A. Faessler, T. Gutsche, and V. E. Lyubovitskij, Strong two-body decays of the $\Lambda_c(2940)^+$ in a hadronic molecule picture, Phys. Rev. D **81**, 014006 (2010).

[21] Y. Dong, A. Faessler, T. Gutsche, S. Kumano, and V. E. Lyubovitskij, Radiative decay of $\Lambda_c(2940)^+$ in a hadronic molecule picture, Phys. Rev. D **82**, 034035 (2010).

[22] J. R. Zhang, S-wave $D^{(*)}N$ molecular states: $\Sigma_c(2800)$ and $\Lambda_c(2940)^+$?, Phys. Rev. D **89**, 096006 (2014).

[23] L. Zhao, H. Huang, and J. Ping, ND and NB systems in quark delocalization color screening model, Eur. Phys. J. A **53**, 28 (2017).

[24] D. Zhang, D. Yang, X. F. Wang, and K. Nakayama, Possible S-wave $ND^{(*)}$ and $N\bar{B}^{(*)}$ bound states in a chiral quark model, arXiv:1903.01207.

[25] E. Klempt and J. M. Richard, Baryon spectroscopy, Rev. Mod. Phys. **82**, 1095 (2010).

[26] V. Crede and W. Roberts, Progress towards understanding baryon resonances, Rep. Prog. Phys. **76**, 076301 (2013).

[27] H. Y. Cheng, Charmed baryons circa 2015, Front. Phys. **10**, 101406 (2015).

[28] H. X. Chen, W. Chen, X. Liu, Y. R. Liu, and S. L. Zhu, A review of the open charm and open bottom systems, Rep. Prog. Phys. **80**, 076201 (2017).

[29] Y. Kato and T. Iijima, Open charm hadron spectroscopy at B-factories, Prog. Part. Nucl. Phys. **105**, 61 (2019).

[30] Y. Huang, J. He, J. J. Xie, and L. S. Geng, Production of the $\Lambda_c(2940)$ by kaon-induced reactions on a proton target, Phys. Rev. D **99**, 014045 (2019).

[31] X. Y. Wang, A. Guskov, and X. R. Chen, $\Lambda_c^*(2940)^+$ photoproduction off the neutron, Phys. Rev. D **92**, 094032 (2015).

[32] H. Y. Cheng and C. K. Chua, Strong decays of charmed baryons in heavy hadron chiral perturbation theory: An update, Phys. Rev. D **92**, 074014 (2015).

[33] J. J. Xie, Y. B. Dong, and X. Cao, Role of the $\Lambda_c^+(2940)$ in the $\pi^- p \to D^- D^0 p$ reaction close to threshold, Phys. Rev. D **92**, 034029 (2015).

[34] O. Romanets, L. Tolos, C. Garcia-Recio, J. Nieves, L. L. Salcedo, and R. G. E. Timmermans, Charmed and strange baryon resonances with heavy-quark spin symmetry, Phys. Rev. D **85**, 114032 (2012).

[35] J. He, Z. Ouyang, X. Liu, and X. Q. Li, Production of charmed baryon $\Lambda_c(2940)^+$ at PANDA, Phys. Rev. D **84**, 114010 (2011).

[36] H. Y. Cheng and C. K. Chua, Strong decays of charmed baryons in heavy hadron chiral perturbation theory, Phys. Rev. D **75**, 014006 (2007).

[37] C. Chen, X. L. Chen, X. Liu, W. Z. Deng, and S. L. Zhu, Strong decays of charmed baryons, Phys. Rev. D **75**, 094017 (2007).

[38] X. H. Zhong and Q. Zhao, Charmed baryon strong decays in a chiral quark model, Phys. Rev. D **77**, 074008 (2008).

[39] H. X. Chen, W. Chen, Q. Mao, A. Hosaka, X. Liu, and S. L. Zhu, P-wave charmed baryons from QCD sum rules, Phys. Rev. D **91**, 054034 (2015).

[40] R. Mizuk *et al.* (Belle Collaboration), Observation of an Isotriplet of Excited Charmed Baryons Decaying to $\Lambda_c\pi$, Phys. Rev. Lett. **94**, 122002 (2005).

[41] B. Aubert *et al.* (*BABAR* Collaboration), Measurements of $\mathcal{B}(\bar{B}^0 \to \Lambda_c^+ \bar{p})$ and $\mathcal{B}(\bar{B}^- \to \Lambda_c^+ \bar{p}\pi^-)$ and studies of $\Lambda_c^+\pi^-$ resonances, Phys. Rev. D **78**, 112003 (2008).

[42] B. Chen, K. W. Wei, X. Liu, and T. Matsuki, Low-lying charmed and charmed-strange baryon states, Eur. Phys. J. C **77**, 154 (2017).

[43] H. Garcilazo, J. Vijande, and A. Valcarce, Faddeev study of heavy baryon spectroscopy, J. Phys. G **34**, 961 (2007).

[44] K. L. Wang, Y. X. Yao, X. H. Zhong, and Q. Zhao, Strong and radiative decays of the low-lying S- and P-wave singly heavy baryons, Phys. Rev. D **96**, 116016 (2017).

[45] Y. Dong, A. Faessler, T. Gutsche, and V. E. Lyubovitskij, Charmed baryon $\Sigma_c(2800)$ as a ND hadronic molecule, Phys. Rev. D **81**, 074011 (2010).

[46] K. Tsushima, D. H. Lu, A. W. Thomas, K. Saito, and R. H. Landau, Charmed mesic nuclei, Phys. Rev. C **59**, 2824 (1999).

[47] C. Garcia-Recio, J. Nieves, and L. Tolos, D mesic nuclei, Phys. Lett. B **690**, 369 (2010).

[48] A. Hosaka, T. Hyodo, K. Sudoh, Y. Yamaguchi, and S. Yasui, Heavy hadrons in nuclear matter, Prog. Part. Nucl. Phys. **96**, 88 (2017).

[49] G. Krein, A. W. Thomas, and K. Tsushima, Nuclear-bound quarkonia and heavy-flavor hadrons, Prog. Part. Nucl. Phys. **100**, 161 (2018).

[50] R. Machleidt, K. Holinde, and C. Elster, The Bonn meson exchange model for the nucleon-nucleon interaction, Phys. Rep. **149**, 1 (1987).

[51] J. Haidenbauer, G. Krein, U. G. Meißner, and A. Sibirtsev, $\bar{D}N$ interaction from meson-exchange and quark-gluon dynamics, Eur. Phys. J. A **33**, 107 (2007).

[52] J. Haidenbauer, G. Krein, U. G. Meißner, and A. Sibirtsev, Charmed meson rescattering in the reaction $\bar{p}d \to \bar{D}DN$, Eur. Phys. J. A **37**, 55 (2008).

[53] J. Haidenbauer, G. Krein, U. G. Meißner, and L. Tolos, DN interaction from meson exchange, Eur. Phys. J. A **47**, 18 (2011).

[54] S. Weinberg, Nuclear forces from chiral Lagrangians, Phys. Lett. B **251**, 288 (1990).

[55] S. Weinberg, Effective chiral Lagrangians for nucleon-pion interactions and nuclear forces, Nucl. Phys. **B363**, 3 (1991).

[56] V. Bernard, N. Kaiser, and U. G. Meißner, Chiral dynamics in nucleons and nuclei, Int. J. Mod. Phys. E **04**, 193 (1995).

[57] E. Epelbaum, H. W. Hammer, and U. G. Meißner, Modern theory of nuclear forces, Rev. Mod. Phys. **81**, 1773 (2009).

[58] R. Machleidt and D. R. Entem, Chiral effective field theory and nuclear forces, Phys. Rep. **503**, 1 (2011).

[59] U. G. Meißner, The long and winding road from chiral effective Lagrangians to nuclear structure, Phys. Scr. **91**, 033005 (2016).

[60] H.-W. Hammer, S. König, and U. van Kolck, Nuclear effective field theory: Status and perspectives, arXiv: 1906.12122.

[61] R. Machleidt and F. Sammarruca, Can chiral EFT give us satisfaction?, Eur. Phys. J. A **56**, 95 (2020).

[62] Z. W. Liu, N. Li, and S. L. Zhu, Chiral perturbation theory and the $\bar{B}\bar{B}$ strong interaction, Phys. Rev. D **89**, 074015 (2014).

[63] H. Xu, B. Wang, Z. W. Liu, and X. Liu, DD^* potentials in chiral perturbation theory and possible molecular states, Phys. Rev. D **99**, 014027 (2019).

[64] B. Wang, Z. W. Liu, and X. Liu, $\bar{B}^{(*)}\bar{B}^{(*)}$ interactions in chiral effective field theory, Phys. Rev. D **99**, 036007 (2019).
[65] L. Meng, B. Wang, G. J. Wang, and S. L. Zhu, The hidden charm pentaquark states and $\Sigma_c\bar{D}^{(*)}$ interaction in chiral perturbation theory, Phys. Rev. D **100**, 014031 (2019).
[66] B. Wang, L. Meng, and S. L. Zhu, Hidden-charm and hidden-bottom molecular pentaquarks in chiral perturbation theory, J. High Energy Phys. 11 (2019) 108.
[67] L. Meng, B. Wang, and S. L. Zhu, $\Sigma_c N$ interaction in chiral perturbation theory, arXiv:1912.09661.
[68] B. Wang, L. Meng, and S. L. Zhu, Spectrum of the strange hidden charm molecular pentaquarks in chiral effective field theory, Phys. Rev. D **101**, 034018 (2020).
[69] S. Scherer, Introduction to chiral perturbation theory, Adv. Nucl. Phys. **27**, 277 (2003).
[70] K. Holinde and R. Machleidt, Effect of the $\Delta(1236)$ resonance on NN scattering, nuclear matter and neutron matter, Nucl. Phys. **A280**, 429 (1977).
[71] H. Krebs, E. Epelbaum, and U. G. Meißner, Nuclear forces with Δ-excitations up to next-to-next-to-leading order, part I: Peripheral nucleon-nucleon waves, Eur. Phys. J. A **32**, 127 (2007).
[72] E. Epelbaum, H. Krebs, and U. G. Meißner, Δ-excitations and the three-nucleon force, Nucl. Phys. **A806**, 65 (2008).
[73] N. Kaiser, S. Gerstendorfer, and W. Weise, Peripheral NN scattering: Role of delta excitation, correlated two pion and vector meson exchange, Nucl. Phys. **A637**, 395 (1998).
[74] T. R. Hemmert, B. R. Holstein, and J. Kambor, Chiral Lagrangians and $\Delta(1232)$ interactions: Formalism, J. Phys. G **24**, 1831 (1998).
[75] M. B. Wise, Chiral perturbation theory for hadrons containing a heavy quark, Phys. Rev. D **45**, R2188 (1992).
[76] A. V. Manohar and M. B. Wise, Heavy quark physics, Camb. Monogr. Part. Phys. Nucl. Phys. Cosmol. **10**, 1 (2000).
[77] E. Epelbaum, W. Glockle, and U. G. Meißner, The two-nucleon system at next-to-next-to-next-to-leading order, Nucl. Phys. **A747**, 362 (2005).
[78] E. Epelbaum, W. Gloeckle, and U. G. Meißner, Improving the convergence of the chiral expansion for nuclear forces. 2. Low phases and the deuteron, Eur. Phys. J. A **19**, 401 (2004).
[79] X. W. Kang, J. Haidenbauer, and U. G. Meißner, Antinucleon-nucleon interaction in chiral effective field theory, J. High Energy Phys. 02 (2014) 113.
[80] E. Epelbaum, H. Krebs, and U. G. Meißner, Improved chiral nucleon-nucleon potential up to next-to-next-to-next-to-leading order, Eur. Phys. J. A **51**, 53 (2015).
[81] D. R. Entem and R. Machleidt, Accurate charge dependent nucleon nucleon potential at fourth order of chiral perturbation theory, Phys. Rev. C **68**, 041001 (2003).
[82] L. Y. Dai, J. Haidenbauer, and U. G. Meiner, Antinucleon-nucleon interaction at next-to-next-to-next-to-leading order in chiral effective field theory, J. High Energy Phys. 07 (2017) 078.
[83] E. Marji, A. Canul, Q. MacPherson, R. Winzer, C. Zeoli, D. R. Entem, and R. Machleidt, Nonperturbative renormalization of the chiral nucleon-nucleon interaction up to next-to-next-to-leading order, Phys. Rev. C **88**, 054002 (2013).
[84] D. R. Entem, R. Machleidt, and Y. Nosyk, High-quality two-nucleon potentials up to fifth order of the chiral expansion, Phys. Rev. C **96**, 024004 (2017).
[85] P. Reinert, H. Krebs, and E. Epelbaum, Semilocal momentum-space regularized chiral two-nucleon potentials up to fifth order, Eur. Phys. J. A **54**, 86 (2018).
[86] T. Yoshida, E. Hiyama, A. Hosaka, M. Oka, and K. Sadato, Spectrum of heavy baryons in the quark model, Phys. Rev. D **92**, 114029 (2015).
[87] D. Ebert, R. N. Faustov, and V. O. Galkin, Masses of excited heavy baryons in the relativistic quark model, Phys. Lett. B **659**, 612 (2008).
[88] S. Q. Luo, B. Chen, Z. W. Liu, and X. Liu, Resolving the low mass puzzle of $\Lambda_c(2940)^+$, Eur. Phys. J. C **80**, 301 (2020).
[89] R. Aaij *et al.* (LHCb Collaboration), Observation of a Narrow Pentaquark State, $P_c(4312)^+$, and of Two-Peak Structure of the $P_c(4450)^+$, Phys. Rev. Lett. **122**, 222001 (2019).
[90] R. Aaij *et al.* (LHCb Collaboration), Observation of $J/\psi p$ Resonances Consistent with Pentaquark States in $\Lambda_b^0 \to J/\psi K^- p$ Decays, Phys. Rev. Lett. **115**, 072001 (2015).
[91] Q. F. Lü, L. Y. Xiao, Z. Y. Wang, and X. H. Zhong, Strong decay of $\Lambda_c(2940)$ as a $2P$ state in the Λ_c family, Eur. Phys. J. C **78**, 599 (2018).
[92] Q. F. Lü and X. H. Zhong, Strong decays of the higher excited Λ_Q and Σ_Q baryons, Phys. Rev. D **101**, 014017 (2020).
[93] X. Z. Weng, L. Y. Xiao, W. Z. Deng, X. L. Chen, and S. L. Zhu, Three body open flavor decays of higher charmonium and bottomonium, Phys. Rev. D **99**, 094001 (2019).
[94] H. Ohki, H. Matsufuru, and T. Onogi, Determination of $B^*B\pi$ coupling in unquenched QCD, Phys. Rev. D **77**, 094509 (2008).
[95] W. Detmold, C. J. D. Lin, and S. Meinel, Calculation of the heavy-hadron axial couplings g_1, g_2, and g_3 using lattice QCD, Phys. Rev. D **85**, 114508 (2012).
[96] E. Epelbaum, U. G. Meißner, W. Gloeckle, and C. Elster, Resonance saturation for four nucleon operators, Phys. Rev. C **65**, 044001 (2002).